Received: 4 June 2016 | Revised: 26 December 2016 | Accepted: 24 May 2017

DOI: 10.1002/stc.2061

RESEARCH ARTICLE

WILEY

Active neural predictive control of seismically isolated structures

Hamid Khodabandolehlou[1] | Gökhan Pekcan[2] | M. Sami Fadali[1] | Mohamed M.A. Salem[3]

[1] Electrical and Biomedical Engineering Department, University of Nevada, Reno, Nevada, USA

[2] Civil and Environmental Engineering Department, University of Nevada, Reno, Nevada, USA

[3] Civil Engineering Department, Helwan University, Cairo, Egypt

Correspondence
Gökhan Pekcan, Civil and Environmental Engineering Department, University of Nevada, Reno, Nevada, USA.
Email: pekcan@unr.edu

Funding information
Departments of Civil and Environmental Engineering; Electrical and Biomedical Engineering

Summary

An online identification and control scheme based on a wavelet neural network (WNN) and model predictive control (MPC) are presented. The WNN comprises a backpropagation neural network with wavelet activation functions and a parallel feedforward term. The WNN is used to identify the structural system, and the model is used to provide the predictions for MPC. The backpropagation network parameters and the controller are trained by the gradient descent algorithm to minimize performance indices. The feedforward component is trained using recursive least squares. The latter is found to drastically reduce the number of hidden layer neurons and significantly reduce the computational load of the neural network. Due to the general structure of the controller, its performance is satisfactory even under the strict condition imposed by a fixed learning rate. The efficacy of the control was demonstrated through a series of computational simulations of a 5-story seismically isolated structure with conventional lead-rubber bearings. Significant reductions of all response amplitudes were achieved for both near-field (pulse) and far-field ground motions, including reduced deformations along with corresponding reduction in acceleration response. In particular, the controller effectively regulated the apparent stiffness at the isolation level.

KEYWORDS

hybrid system, near-field earthquake, neural predictive control, seismic isolation

1 | INTRODUCTION

Seismic isolation is recognized as one of the most effective mitigation strategies for structural and nonstructural systems.[1,2] In general, seismic isolation systems shift the fundamental period of the isolated structure away from the range of predominant excitation periods, which results in reduced acceleration demand. However, as a result of the lengthened period, the base displacement of the isolated system becomes larger and, in some cases, may lead to instability of the isolation system. This issue arises in case of near-field ground motions, which are dominated by long-period velocity pulses. For the case of long period structures, the velocity pulse tends to develop large displacements.[3] The pulse displacement is usually associated with the fault-normal direction, where high spectral acceleration components are observed in the long period range.[4] These long period spectral acceleration components tend to resonate with conventionally isolated structures, leading to an excessive base displacement that may destabilize the structure. To maintain the isolation deformations to within acceptable limits, two potential alternatives are to increase the effective stiffness of the isolation system or to provide additional damping mechanisms. However, increasing the stiffness is counterintuitive. For this reason, many of the isolation systems provide various sources of damping mechanism to overcome the unacceptably large isolation deformations.[5] This damping may be provided by the isolator directly or by means of supplemental damping devices. However, increasing the damping capacity of the isolated structures by means of supplementary dampers leads to an increase in the superstructure's accelerations and interstory drifts.[6] In such circumstances,

conventional seismic isolation systems alone, such as rubber bearings and friction pendulum, may not be the best alternative for seismic response mitigation.

Various alternative hybrid strategies have been proposed and studied analytically and experimentally to overcome the shortcomings of the conventional seismic isolation system (e.g., large isolator deformations). Some of these strategies combine conventional isolation system with actively or semiactively controllable devices.[7–16] Furthermore, control strategies using adaptive neural networks and their application in various types of structural systems, including seismically isolated structures, have been extensively studied during the last two decades.[17–24] Although varying levels of response reduction have been demonstrated by means of active control strategies, there is still a need to develop efficient, consistent, and robust techniques to address the issues stated earlier.

Despite the availability of various adaptive control methods, their application requires an accurate mathematical model of the system.[25] However, model uncertainty or unmodeled dynamics in real-world applications can cause a deterioration in the performance of model-based control systems. This makes model-free methods more attractive. Artificial neural networks can accurately approximate nonlinear systems and have therefore received considerable attention in the identification of nonlinear systems. Han et al.[26] designed a generalized predictive controller for a second-order nonlinear system based on a feedforward neural network identifier. Their simulation results show that neural network control is robust and can meet the design specifications.

The main drawbacks of neural networks are their slow convergence rate, multilayer structure, and computational complexity. Zhang and Beneveniste[27] proposed wavelet networks to eliminate or mitigate these disadvantages. Wavelet networks use wavelets with different scale and shift parameters as activation functions and are thus a good alternative to neural networks for identification of nonlinear systems. They also argued that in higher dimensional problems, wavelet networks typically have fewer hidden layer nodes than other neural networks.

The published research on the development and application of wavelet neural network controllers and system identification is abundant. Sousa et al.[28] identified the model of a robot using a wavelet network and used the identified model to design a dynamic controller. They proved the stability of their controller using the second method of Lyapunov. They argued that in spite of the difficulty of their design and stability analysis, wavelet network controllers provide more flexibility than standard adaptive control approaches. Zayeni and Ahmadi[29] applied a radial wavelet network to the identification of nonlinear system. The structure and learning method of their network are similar to those of radial basis function networks, but their activation functions are wavelets. Simulation results show that these networks can identify models of complex nonlinear systems. Khodabandehlou and Fadali[30] used wavelet network and generalized predictive controller for online identification and networked control of an unmanned vehicle. Their simulation results show satisfactory performance under fixed and random network delay. For more publications on the application of wavelet networks to system identification and control, interested readers are referred to previous studies.[23,31–34]

This study proposes a new model predictive controller (MPC) that uses a wavelet neural network for output identification of nonlinear dynamics and uses it for MPC control of seismically isolated structures. The wavelet neural network includes a back propagation neural network and a feedforward term trained using recursive least squares. This configuration reduces the number of hidden layer nodes significantly. The computational complexity of the error backpropagation algorithm is $O(n^3)$ with n hidden layer nodes. Consequently, reducing n reduces the computational complexity of the wavelet neural network drastically and allows its utilization in online identification and control. This parallel configuration is, to the best of our knowledge, new and is one of the main contributions of this paper. In addition, this paper presents the first application of this new configuration to seismically isolated structures. The approach is applied computationally to the control of a seismically isolated five-story structure subjected to ground motions with both far-field (FF) and near-field (NF) characteristics. Simulation results demonstrate that significant reductions of all response amplitudes were achieved particularly for near-field (pulse) ground motions, including reduced deformations along with corresponding reduction in acceleration response.

2 | WAVELET NEURAL NETWORK

Model predictive control relies on using an accurate system model to predict future outputs. In cases where such a model is not available, system identification becomes an essential part of model predictive control. In this study, a three-layer wavelet neural network in parallel with a feedforward component trained using the recursive least squares (RLS) algorithm is used to identify the model parameters. The RLS algorithm establishes a linear relationship between the inputs and outputs, and the wavelet neural network minimizes the identification error. Figure 1 depicts the structure of the wavelet neural network.

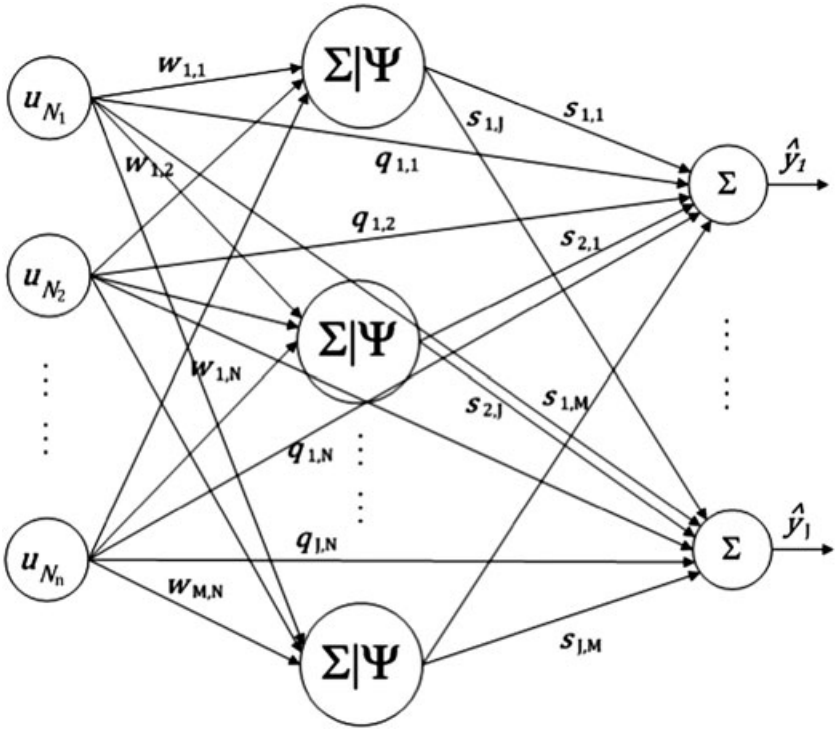

FIGURE 1 Wavelet neural network structure

The input–output equation of the network can be expressed as

$$\hat{y}_j(k) = \sum_{i=1}^{J} s_{j,i} \sum_{t=1}^{n} \psi\left(w_{i,t} \times \mathrm{u_{Nt}} - p_i\right)/r_{i,i}) + \sum_{t=1}^{n} q_{j,t} \times \mathrm{u_{Nt}} \ , 1 \le j \le J \tag{1}$$

$$\hat{\mathrm{y}}(k) = [\,\hat{y}_1(k), \hat{y}_2(k), \ldots, \hat{y}_J(k)]^T, \tag{2}$$

where $\hat{\mathbf{y}}$ is the network output and $\mathbf{u}_N = [\mathrm{u}_{Nt}]$ is the $n \times 1$ network input vector. Assuming that the network has J outputs and m hidden layer nodes, $\mathbf{S} = [s_{i,j}]$ is a $J \times m$ matrix, $\mathbf{W} = [w_{i,j}]$ is $m \times n$ matrix, $\mathbf{p} = [p_i]$ is $m \times 1$ vector, and $\mathbf{R} = [r_{i,j}]$ is a $m \times m$ diagonal matrix whose diagonal elements are positive, and off-diagonals are zero and $\mathbf{Q} = [q_{i,j}]$ is $J \times n$ matrix. The activation function of the hidden layer nodes, ψ, is

$$\psi_{p,r} = \psi\left(\frac{t-p}{r}\right). \tag{3}$$

The activation function is chosen to be the Mexican hat wavelet

$$\psi(t) = \frac{2\pi^{\frac{1}{4}}}{\sqrt{3}}\left(1-t^2\right)e^{-\frac{t^2}{2}}. \tag{4}$$

The well-known error back propagation algorithm is used to train the wavelet neural network weights, whereas **Q** is trained using the RLS algorithm. RLS learns the behavior of the system much faster than the wavelet network and traditional neural networks. Consequently, the wavelet neural network learns the behavior of the system faster, which makes the model more appropriate for online identification and control. In addition, particularly when the system behavior is approximately linear under certain operating conditions, the parallel configuration drastically reduces the number of hidden layer nodes for specified accuracy. Consequently, the training time of the WNN drops significantly making the algorithm more efficient for real time applications. The reduction of the number of hidden layer nodes for specified approximation accuracy reduces model complexity without sacrificing accuracy.

The cost function for training the network parameter is assumed to be sum of squared errors

$$J(k) = \frac{1}{2}\sum_{k=1}^{N}\sum_{j=1}^{m}\left(\hat{y}_j(k) - y_j(k)\right)^2, \tag{5}$$

where $y_j(k)$ is the jth output of the system and $\hat{y}_j(k)$ is the jth output of the wavelet neural network at time step k. The gradient descent method is used to update the network parameters

$$\sigma_{k+1} = \sigma_k - \gamma\frac{\partial J(k)}{\partial \sigma_k}, \tag{6}$$

where γ is the gradient descent algorithm learning rate. By defining the partial error as

$$e_{y_j}(k) = \hat{y}_j(k) - y_j(k) - \sum_{t=1}^{n} q_{j,t}\mathbf{u}_{Nt}. \tag{7}$$

The change in each parameter can be calculated using the chain rule as[27,28,30]

$$\frac{\partial J}{\partial \sigma_k} = \sum_{j=1}^{J} e_{y_j}(k)\frac{\partial \hat{y}_j(k)}{\partial \sigma_k}. \tag{8}$$

3 | WAVELET NEURAL NETWORK BASED MPC

Predictive control uses an explicit model of the system to predict future outputs of the system and uses them to calculate future inputs. It assumes that the inputs and outputs of the system can be measured and used to update the network parameters. In each iteration, the controller updates the network parameters and uses the wavelet neural network to predict future outputs over a prediction horizon N_p, then calculates the future inputs over a control horizon $N_u \le N_p$ by minimizing the cost function

$$J_c = \frac{1}{2}\sum_{i=1}^{N_p}\sum_{j=1}^{m} l_j e_{y_j,c}(k+i)^2 + \frac{1}{2}\sum_{i=1}^{N_u}\rho\Delta \mathrm{u}(k+i-1)^2, \tag{9}$$

where $e_{y_j,c}(k+i)$ is the error between desired value and predicted value of the jth output of the system at time $k+i$ and l_j is penalty on this error, $\Delta\mathbf{u}$ is the change in the control input, and ρ is the penalty on the change in the control input.

Because the desired accelerations and displacements are zero, minimizing prediction error is equivalent to minimizing the response of the system. To avoid excessive control force, a penalty on control force increments is included in the cost function. A long control horizon leads to a smooth and small control input but decreases the tracking performance. A long prediction horizon leads to smooth control input also but decreases the tracking speed.

The controller cost function J_c can be written in terms of the control as

$$J_c = \frac{1}{2}\left[\sum_{j=1}^{J}\left(\mathbf{e}_{y_j,c}^{T}(k+1)\mathbf{L}\mathbf{e}_{y_j,c}(k+1)\right) + \rho(\mathbf{H}\mathbf{u}(k))^T(\mathbf{H}\mathbf{u}(k))\right], \tag{10}$$

in which $\mathbf{L}$ is a diagonal matrix with l_j's as its diagonal elements and

$$\mathbf{H} = \begin{bmatrix} 1 & 0 & 0 & \dots & 0 \\ -1 & 1 & 0 & \dots & 0 \\ 0 & -1 & 1 & \dots & 0 \\ 0 & \dots & \ddots & \ddots & 0 \\ 0 & \dots & 0 & -1 & 1 \end{bmatrix}, \tag{11}$$

$$\mathbf{e}_{y_j,c}(k+1) = \mathbf{y}_{j_d}(k+1) - \hat{\mathbf{y}}_j(k+1) \;\; , 1 \le j \le J, \tag{12}$$

where y_{jd} is the desired value of the jth output and $\hat{y}_j$ is its predicted value as follows:

$$\mathbf{y}_{j_d}(k+1) = \left[y_{jd}(k+1), \ldots, y_{jd}\left(k+N_p\right)\right]^T \ , 1 \le j \le J, \tag{13}$$

$$\hat{\mathbf{y}}_j(k+1) = \left[\hat{y}_j(k+1), \ldots, \hat{y}_j\left(k+N_p\right)\right]^T, 1 \le j \le J, \tag{14}$$

$$\mathbf{u}(k) = [u(k), u(k+1), \ldots, u(k+N_u - \ 1)]^T, 1 \le i \le m. \tag{15}$$

The change in control input can be calculated by optimizing J_c via gradient descent based on the following generalized form:

$$\frac{\partial J_c}{\partial \boldsymbol{u}(k)} = -\sum_{j=1}^{J} \mathbf{G}_{y_j,u}^T \mathbf{Le}_{y_j,c}(k+1), \tag{16}$$

$$\Delta\mathbf{u}(\mathrm{k}) = \left(I + \lambda\rho\mathbf{H}^T\right)^{-1} \times \frac{\partial J_c}{\partial \mathbf{u}(k)} \ \ and \ \ \mathbf{u}(k+1) = \mathbf{u}(k) + \Delta\mathbf{u}(\mathrm{k}), \tag{17}$$

$$\mathbf{G}_{\mathbf{y}_j,u} \ = \left[g_{y_j,u}(s,l)\right] \ such \ that \ g_{\mathbf{y}_j,u}(s,l) = \begin{cases} \dfrac{\partial \hat{y}_j(k+s)}{\partial u(k+l-1)} & , s \ge l \\ 0 & , s < l \end{cases}$$

$$1 \le j \le J, 1 \le s \le N_p, 1 \le l \le N_u, \tag{18}$$

where λ is the learning rate of the gradient descent algorithm.[25,30] All the derivatives are calculated using the chain rule

$$\frac{\partial \hat{y}_j(k+q)}{\partial u(k+r)} = \frac{\partial \hat{y}_j(k+q)}{\partial \hat{y}_j(k+q-1)} \times \frac{\partial \hat{y}_j(k+q-1)}{\partial \hat{y}_j(k+q-2)} \times \ldots$$

$$\ldots \times \frac{\partial \hat{y}_j(k+r+2)}{\partial \hat{y}_j(k+r+1)} \times \frac{\partial \hat{y}_j(k+r+1)}{\partial u(k+r)}. \tag{19}$$

3.1 | Alternative controllers

A benchmark comparison of the proposed WNN-based controller is demonstrated with respect to linear quadratic Gaussian (LQG) and multivariable proportional-integral (PI) controllers. LQG control assumes that enough state variables of the structure, that is enough velocities and displacements, can be measured to make the system observable. The measurements are fed to a Kalman filter, which estimates the states and control inputs of the system. In practice, accelerations are the only measured variables, and velocities and displacements are obtained by integrating the accelerations. Integration introduces errors in the inputs to the Kalman filter and reduce the quality of LQG control.

Designing a PI controller for single-input–multi-output systems is a challenging problem. The system must be completely controllable, whereas the seismically isolated structural model has five uncontrollable modes. To overcome this, Kalman decomposition is used to find the controllable subsystem of the structure. The controllable subsystem of the structure is a single-input–six-output system. A multivariable PI controller is then designed for the controllable subsystem using linear quadratic methods. Details of the two controllers are available in Anderson and Moore[35] and are omitted for brevity. The response of an actively controlled five-story seismically isolated simulation model with different controllers is presented in Section 5 and in Table 3.

4 | COMPUTATIONAL SIMULATION MODEL

The computational simulation model represents the five-story seismically isolated structure that was developed for an experimental program by Kelly and Tsai[36] as shown in Figure 2. The model was analyzed as a conventionally isolated structure with lead-rubber bearings (LRB) only, and with LRBs coupled with actuators that provide the active control forces. In general, various types of devices may be employed in active control. Although a specific type has not been assumed nor modeled, the most suitable devices in these types of applications may be hydraulic (or electrical) actuators. The lumped system properties are summarized in Table 1. The postyield stiffness, k_b, of the isolation system was originally selected so that the fundamental period of the structure is 2.5 s once the lead plug yields. The characteristic strength, Q_y, is selected to be 10% of the building's weight, and the postyield to preyield stiffness ratio, α, is taken as 8.5%. These values were recommended by Ramallo et al.[37] to achieve acceptable control of the base displacement without excessive structural accelerations for both moderate and severe seismic events. The inherent damping of the structure is assumed to be 2%.

4.1 | Equations of motion

The all-inclusive equations of motion of the seismically isolated structure (Figure 2) can be written as

$$\mathbf{M}_s\,\ddot{\mathbf{u}}_s^t + \mathbf{C}_s\,\dot{\mathbf{u}}_s + \mathbf{K}_s\,\mathbf{u}_s = 0, \tag{20}$$

$$m_b\ddot{u}_b^t + F_d(c_b(t), \dot{u}_b) + F_s(\alpha(t), u_b, \dot{u}_b, z) - \mathbf{I}_s^T\,\mathbf{V}_s = 0, \tag{21}$$

in which $\mathbf{M}_s$, $\mathbf{C}_s$, and $\mathbf{K}_s$ are the mass, damping, and stiffness matrices of the superstructure, respectively. Equation 20 governs the superstructure motion, whereas Equation 21 defines the base slab motion. Furthermore, m_b is the base slab mass,

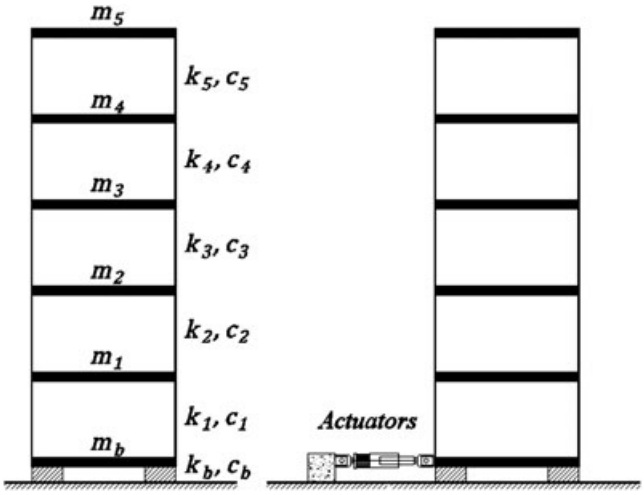

FIGURE 2 Simulation model, (a) LRB isolated, (b) LRB isolated and controlled

TABLE 1 Properties of the simulation model

Floor mass (kg)	Stiffness coefficients (kN/m)	Damping coefficients (kN•s/m)
$m_b = 6{,}800$	$k_b = 232$	$c_b = 3.74$
$m_1 = 5{,}897$	$k_1 = 33{,}732$	$c_1 = 67$
$m_2 = 5{,}897$	$k_2 = 29{,}093$	$c_2 = 58$
$m_3 = 5{,}897$	$k_3 = 28{,}621$	$c_3 = 57$
$m_4 = 5{,}897$	$k_4 = 24{,}954$	$c_4 = 50$
$m_5 = 5{,}897$	$k_5 = 19{,}059$	$c_5 = 38$

$F_d(c_b(t), \dot{u}_b)$, and $F_s(\alpha(t), u_b, \dot{u}_b, z)$ are the damping force and the restoring force of the substructure (isolation level), respectively. The damping force term F_d is provided for cases where additional source of damping at the isolation level might be considered. $\ddot{\mathbf{u}}_s$, $\dot{\mathbf{u}}_s$, and $\mathbf{u}_s$ are the acceleration, velocity, and displacement vectors of the superstructure with respect to the base slab, respectively, and $\ddot{u}_b, \dot{u}_b$, and u_b are those of substructure with respect to the ground. The superscript, t, denotes the total displacement with respect to a fixed reference. $\mathbf{I}_s$ is the influence array of the superstructure motion on the substructure motion, and $\mathbf{V}_s$ is the vector of shear forces induced on the superstructure:

$$\mathbf{V}_s = -\mathbf{M}_s \ddot{\mathbf{u}}_s^t. \tag{22}$$

The total displacement vectors can be expressed as

$$\mathbf{u}_s^t = \mathbf{u}_s + \mathbf{I}_b u_b + \mathbf{I}_1 u_g, \tag{23}$$

$$u_b^t = u_b + \mathbf{I}_2 u_g, \tag{24}$$

where $\mathbf{I}_b$ is the influence array of the base slab motion on the DOFs of the superstructure, $\mathbf{I}_1$ and $\mathbf{I}_2$ are the influence arrays of the ground motion on the superstructure and base slab DOFs, respectively, and u_g is the total ground displacement. Substituting for $\mathbf{u}_s^t$ and u_b^t and rearranging, the governing equations of motion can be written as

$$\mathbf{M}_s \ddot{\mathbf{u}}_s \ + \mathbf{C}_s \dot{\mathbf{u}}_s + \mathbf{K}_s \mathbf{u}_s = -\mathbf{M}_s \left(\mathbf{I}_b \ddot{u}_b + \mathbf{I}_1 \ddot{u}_g \right), \tag{25}$$

$$m_b \ddot{u}_b + F_d(c_b, \dot{u}_b) + F_s(\alpha, u_b, \dot{u}_b, z) = -m_b \mathbf{I}_2 \ddot{u}_g - \mathbf{I}_s^T \mathbf{M}_s \left(\ddot{\mathbf{u}}_s \ + \mathbf{I}_b \ddot{u}_b + \mathbf{I}_1 \ddot{u}_g \right). \tag{26}$$

The restoring force $F_s(\alpha, u_b, \dot{u}_b, z)$ represents the true hysteresis behavior of conventional LRB isolation systems. The well-known Bouc-Wen model[38] has been used in this study:

$$F_s = k_b u_b + (1-\alpha) k_e x_y z, \tag{27}$$

$$\dot{z} = A\dot{u}_b - \beta |\dot{u}_b| z |z|^{n-1} - \gamma \dot{u}_b |z|^n, \tag{28}$$

where α is the ratio of the postyield to the preyield stiffness of the isolation system, x_y is the yield displacement of the isolators, z is dimensionless parameter that defines the hysteresis of the isolation system, and n, A, β, and γ are constant parameters that control the shape of the hysteresis loops. The parameter z is found by solving the nonlinear differential Equation 28. For the elastic stiffness to be modeled properly ($A = \beta + \gamma$), and for the unloading to follow the elastic stiffness ($\beta = \gamma$). Equations 25 and 26 can be written in matrix form

$$\overbrace{\begin{bmatrix} \mathbf{M_s} & \mathbf{M_s I_b} \\ \mathbf{I}_s^T \mathbf{M}_s & m_b + \mathbf{I}_s^T \mathbf{M}_s \mathbf{I_b} \end{bmatrix}}^{\bar{\mathbf{M}}} \begin{bmatrix} \ddot{\mathbf{u}}_s \\ \ddot{u}_b \end{bmatrix} + \overbrace{\begin{bmatrix} \mathbf{C}_s & 0 \\ 0 & c_b \end{bmatrix}}^{\bar{\mathbf{C}}} \begin{bmatrix} \dot{\mathbf{u}}_s \\ \dot{u}_b \end{bmatrix} + \overbrace{\begin{bmatrix} \mathbf{K}_s & 0 \\ 0 & k_b \end{bmatrix}}^{\bar{\mathbf{K}}} \begin{bmatrix} \boldsymbol{u}_s \\ u_b \end{bmatrix} = \overbrace{\begin{bmatrix} -\mathbf{M_s I}_1 \\ -m_b \mathbf{I}_2 - \mathbf{I}_s^T \mathbf{M}_s \mathbf{I}_1 \end{bmatrix}}^{\mathbf{E}_g} \ddot{u}_g + \overbrace{\begin{bmatrix} 0 \\ -\mathbf{I_c} \end{bmatrix}}^{\mathbf{E}_c} f_c, \tag{29}$$

where $\mathbf{I}_c$ is the location matrix of the restoring force of the isolation system and the control force. Equation 29 can be represented in state space as

$$\dot{\mathbf{x}} = \mathbf{A}\mathbf{x} + \mathbf{B} f_c + \mathbf{E} \ddot{u}_g, \tag{30}$$

$$\mathbf{y} = \mathbf{C}_y \mathbf{x} + \mathbf{D}_y f_c + \mathbf{E}_y \ddot{u}_g + \mathbf{v}, \tag{31}$$

where $\mathbf{x} = \left[\boldsymbol{u}_s^T, u_b, \dot{\boldsymbol{u}}_s^T, \dot{u}_b \right]^T$ is the state vector, $\mathbf{y}$ represents the vector of measurements, and $\mathbf{v}$ is the measurement noise. The state matrices are defined as

$$\mathbf{A} = \begin{bmatrix} 0 & \boldsymbol{I} \\ -\widetilde{\mathbf{M}}^{-1} \widetilde{\mathbf{K}} & -\widetilde{\mathbf{M}}^{-1} \widetilde{\mathbf{C}} \end{bmatrix}, \qquad \mathbf{B} = \begin{bmatrix} 0 \\ \widetilde{\mathbf{M}}^{-1} \mathbf{E}_c \end{bmatrix}, \ \mathbf{E} = \begin{bmatrix} 0 \\ -\widetilde{\mathbf{M}}^{-1} \mathbf{E}_g \end{bmatrix}, \tag{32}$$

and C_y, D_y, and E_y are obtained from the measured state. Assuming that the floor and base slab accelerations are measured:

$$\mathbf{C}_y = \left[-\bar{\mathbf{M}}^{-1}\tilde{\mathbf{K}} \;\; -\bar{\mathbf{M}}^{-1}\tilde{\mathbf{C}}\right], \mathbf{D}_y = \left[-\bar{\mathbf{M}}^{-1}\mathbf{E}_c\right], \mathbf{E}_y = 0, \bar{\mathbf{M}} = \begin{bmatrix} \mathbf{M}_s & 0 \\ \mathbf{I}_s^T \boldsymbol{M}_s & m_b \end{bmatrix}. \tag{33}$$

In case of passive isolators, $(f_c = (1-\alpha)k_e x_y z)$ represents the hysteretic behavior; otherwise, the control force is superimposed on f_c. The state of the structure is used to generate its input–output data for identification and to update the parameters of the wavelet neural network as described earlier.

The computational simulation of both the uncontrolled (seismically isolated with conventional LRBs) and the controlled (with or without LRBs) structure are performed using Matlab/Simulink.[39] A block diagram of the online identification and control implementation is shown schematically in Figure 3.

The neural network input vector includes the control force and the history of acceleration. The input to the network is defined as

$$\mathbf{u}_N(k) = [f_c(k-1), \mathbf{y}(k-1), \ldots, \mathbf{y}(k-10)], \tag{34}$$

where $\mathbf{y}$ is a 6×1 vector of accelerations:

$$\mathbf{y}(\mathrm{k}) = [y_1(k), y_2(k), \ldots, y_6(k)]^T. \tag{35}$$

For the simulations in this study, 10 hidden layer neurons and a fixed learning rate of $\gamma = 0.2$ were specified. Both the prediction horizon N_p and the control horizon N_u were set equal to 10. The control input weighting factors for different cases investigated were chosen as $\rho = 10^{-1}$ for a medium-level penalty on the acceleration response, and $\rho = 10^{-4}$ for high penalty on the acceleration response. Because the accelerations along the height of the base isolated structure are approximately equal, the weight matrix L for the output prediction error is the identity matrix to impose the same penalty on all of the accelerations. The neural network parameters are randomly initialized except for setting the matrix $\mathbf{R}$ equal to the identity and the vector $\mathbf{q}$ equal to zero.

Because the RLS algorithm can quickly establish a linear relationship between inputs and outputs, no pretuning is needed on the WNN. However, for real world applications, the number of hidden layer nodes can be effectively predetermined using an approximate computational simulation model of the structure.

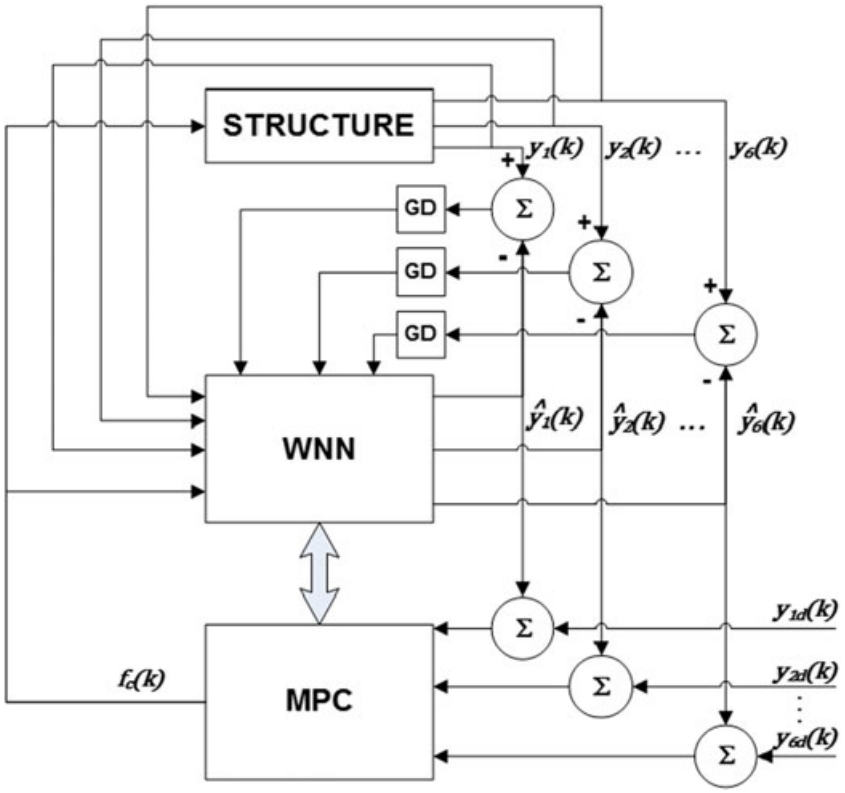

FIGURE 3 Block diagram of the online identification and control scheme. MPC = model predictive control; WNN = wavelet neural network

Last but not the least, for accurate system identification, the excitation should be sufficiently large to excite significant modes of vibration of the system, which is always the case for high-intensity ground motions of interests. However, a key factor that may affect the performance of controller implementation is the noise in output measurements. Therefore, the simulations were repeated for two cases, with and without measurement noise to demonstrate the robustness of the proposed control strategy in that regard. Robustness with respect to variations in system parameters (structural stiffness, isolation properties, etc.) is not considered in this paper because the nonlinearities are assumed to be only associated with the isolation bearings. However, a more comprehensive assessment is part of an ongoing study that investigates full-scale implementation of the proposed control strategy, including the effects of variations in system parameters.

4.2 | Ground motions

To illustrate the effectiveness of the proposed WNN-based control implementation, the seismically isolated structure is subjected to a series of recorded far-field and near-field ground motions. Seven far-field and seven near-field [pulse] type recorded ground motions are selected as summarized in Table 2, and 5% damped acceleration response spectra are plotted in Figure 4. The ground motions were selected as a subset of FEMA P695 records.[40] The ground motions were neither time-scaled nor amplitude-scaled because the main purpose of the study is to provide a relative comparison of achieved controlled response versus conventional seismic isolation. Selected ground motions in the near-field [pulse] type group were targeted to have peak ground velocities (PGV) greater than 100 cm/s (with one exception; 1992 Erzincan) and peak ground acceleration (PGA) to PGV ratios less than 0.7 g/m/s. For the far-field type ground motions, the corresponding targets were PGV $\geq$ 40 cm/s and PGA/PGV$\leq$1.2 g/m/s. Whereas both [high] PGV and [low] PGA/PGV parameters are considered as "damage" indicators, the average PGAs of the two sets of ground motions were selected to be comparable; 0.55 g (FF) versus 0.60 g (NF).

5 | PERFORMANCE OF CONVENTIONAL AND CONTROLLED STRUCTURES

In the simulation, the only observable responses were assumed to be floor and isolation level accelerations as indicated in Equations 31 through 34. Therefore, the penalty factor ρ that is used in the minimization of the control cost function J_c applies to the measured acceleration response in Equation 10. Smaller ρ values imply smaller desired acceleration response. Furthermore, WNN-based control does not require real-time simulation of the structure. However, a feasible weight ρ, learning rate λ, and the number of hidden layer nodes m are determined offline using an approximate simulation model before implementation. These

TABLE 2 Details of the ground motion records

Equation ID	Record name	M_w	Recording station	Dur. (s)	R (km)	PGA (g)	PGV (cm/s)	PGD (cm)
Far-field (FF) ground motions								
F01	01-Northridge, 1994	6.7	Beverly Hills-Mul.	23.95	13.3	0.62	40.7	8.56
F02	02-Northridge, 1994	6.7	Canyon Count.-WLC	19.95	26.5	0.48	44.9	12.5
F03	03-Duzce, Turkey, 1999	7.1	Bolu	55.85	41.3	0.82	62.1	13.6
F04	06-Imperial Valley, 1979	6.5	El Centro Array 11	39.03	29.4	0.38	42.1	18.6
F05	12-Landers, 1992	7.3	Coolwater	27.96	82.1	0.42	42.3	13.8
F06	18-Cape Mendocino, 1992	7.0	Rio Dell Overpass	35.90	22.7	0.55	41.9	19.5
F07	20-Chi-Chi, Taiwan, 1999	7.6	TCU045	89.98	77.5	0.51	40.0	14.3
Near-field (NF) with pulse ground motions								
N01	02-Imperial Valley, 1979	6.5	El Centro Array 7	36.80	27.6	0.46	109.3	44.7
N02	04-Superstition Hills, 1987	6.5	Parachute Test Site	22.30	16.0	0.45	111.9	52.8
N03	06-Erzincan, Turkey, 1992	6.7	Erzincan	21.30	9.00	0.52	95.5	27.7
N04	09-Northridge, 1994	6.7	Rinaldi Receiving	14.93	10.9	0.83	166.0	28.1
N05	10-Northridge, 1994	6.7	Sylmar—Olive View	39.90	16.8	0.84	129.4	39.9
N06	12-Chi-Chi, Taiwan, 1999	7.6	TCU065	89.98	26.7	0.81	126.2	92.6
N07	13-Chi-Chi, Taiwan, 1999	7.6	TCU102	89.98	45.6	0.30	112.5	89.2

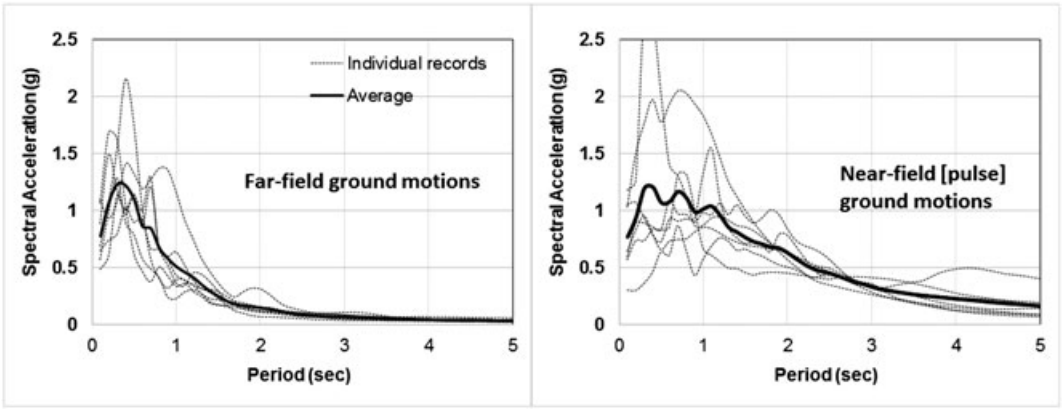

FIGURE 4 Response spectra of the selected ground motions

parameters are fixed during real time application, and the network weights are the only parameters that are updated every time step. In this study, first, a lower bound $\rho = 10^{-4}$ was selected to examine the efficacy of the control method to reduce accelerations irrespective of the associated displacements. This is referred to as the *Cont-C2* case. In an attempt to reduce displacements while maintaining accelerations, base shear, and foundation shear forces under acceptable limits, a larger $\rho = 10^{-1}$ was used. This case is referred to as *Cont-C1*.

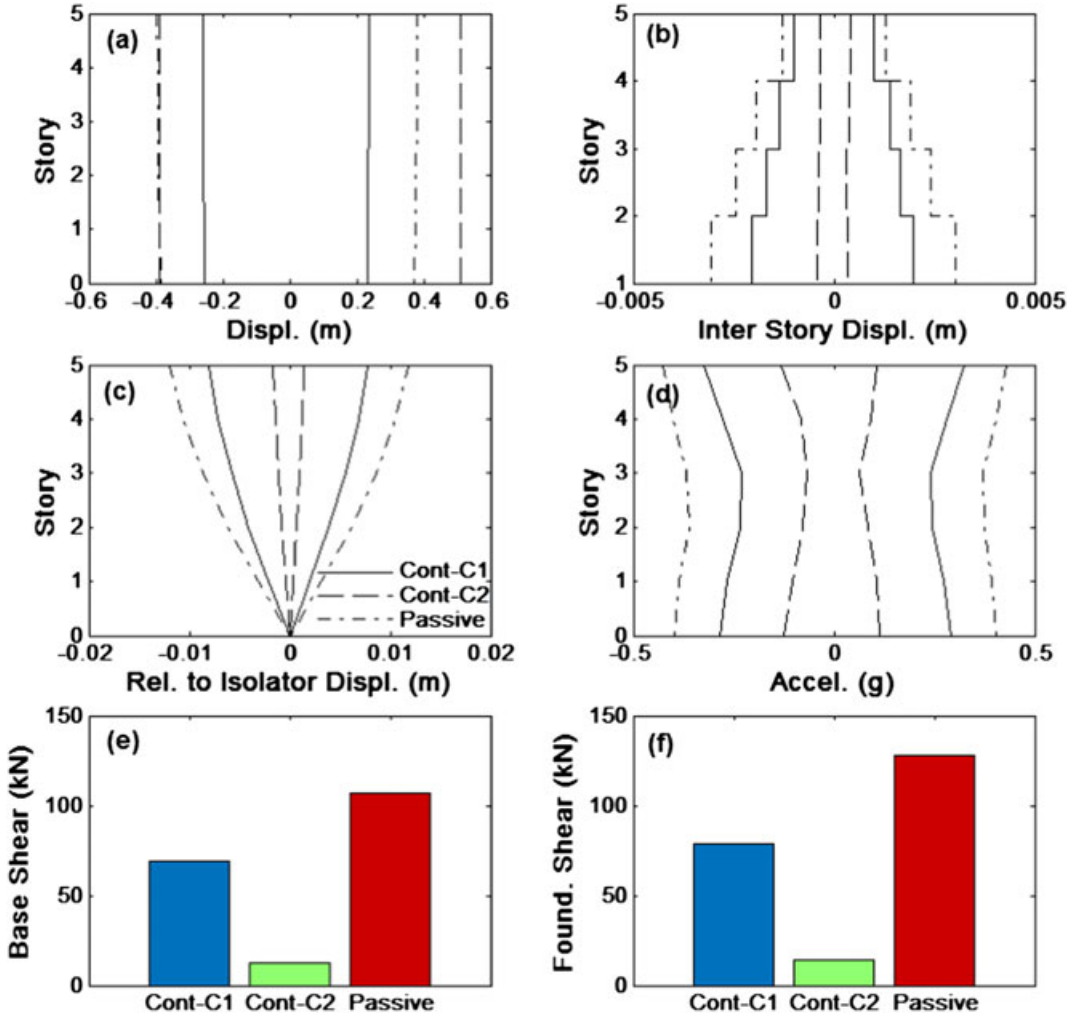

FIGURE 5 Comparison of average maximum response—near-field ground motions. (a) Story and base [isolator] displacements, (b) interstory drifts, (c) displacements relative to isolator, (d) story and base [isolator level] accelerations, (e) [superstructure] base shear, (f) sum of isolator force and control force (if any)

Thus, the three different cases investigated are (a) conventional seismically isolated structure with LRBs (*Passive*), (b) structure with LRBs coupled with control with high penalty on acceleration response (*Cont-C2*; $\rho = 10^{-4}$), and (c) structure with LRBs coupled with control with medium-level penalty on acceleration response (*Cont-C1*; $\rho = 10^{-1}$). Each case was subjected to both NF and FF ground motions. A summary of the simulation results is presented in Figure 5 and Figure 9 for the NF and FF ground motions, respectively. These figures present the average of maximum (a) floor and base [isolator] displacements, (b) interstory drifts, (c) displacements relative to isolator, (d) floor and base accelerations, (e) [superstructure] base shear, and (f) total shear force at the foundation level, which includes the isolator force and control force for the controlled cases.

As can be seen in Figure 5(a–d), the overall displacement response is reduced by an average of 40% in the *Cont-C1* case with similar reductions in acceleration response along the height of the structure in comparison to the *Passive* case. In particular, the simultaneous reduction in the base displacement and the floor accelerations under pulse-type NF ground motions is notable. Sample displacement response history comparisons for two of the NF ground motions are shown in Figure 6 where the pulse-type nature of the earthquakes is evident. The simulation results demonstrate that *Cont-C2* implementation reduces the resonance behavior of the seismic isolation system induced by long-period ground motions. Although the initial displacement pulse was not reduced significantly, subsequent larger isolation deformations were mitigated. These response reductions are achieved by the control force which effectively regulates the apparent isolation stiffness in real time (Figure 7). Furthermore, reduced floor accelerations result in lower superstructure base shear as well as foundation forces (Figure 5e,d).

The *Cont-C2* case employs a low weight ρ for control input with an objective to completely attenuate the acceleration response. As shown in Figure 5, this objective was achieved to the extent possible, which further resulted in significantly

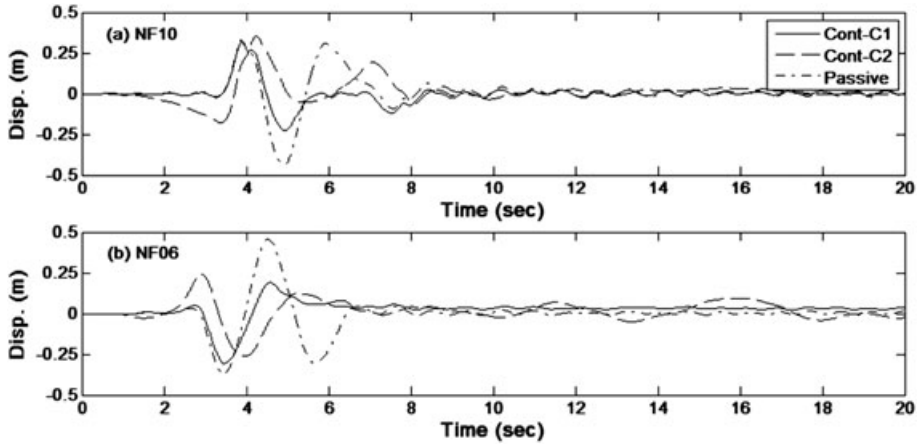

FIGURE 6 Sample isolator displacement response history comparisons. (a) NF05, (b) NF03

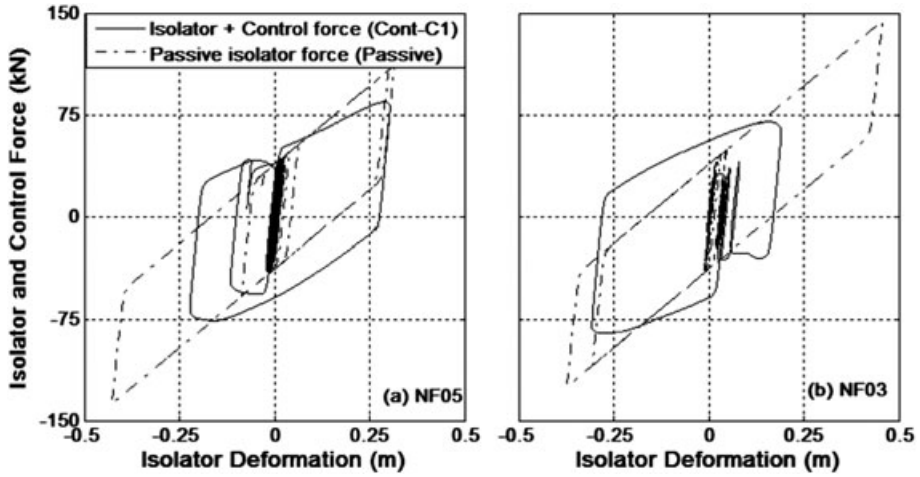

FIGURE 7 Sample isolator deformation versus isolator/control force deformation response. (a) NF05, (b) NF03

reduced interstory drifts and base shear forces, albeit at the expense of larger isolator deformations compared to *Cont-C1* and *Passive* cases. In theory, the floor accelerations would tend to zero as the effective stiffness at the base of the structure reduces to zero. Our simulations show that WNN control dictates out-of-phase control forces with respect to isolator forces, which results in essentially zero effective stiffness in the isolation system (Figure 8).

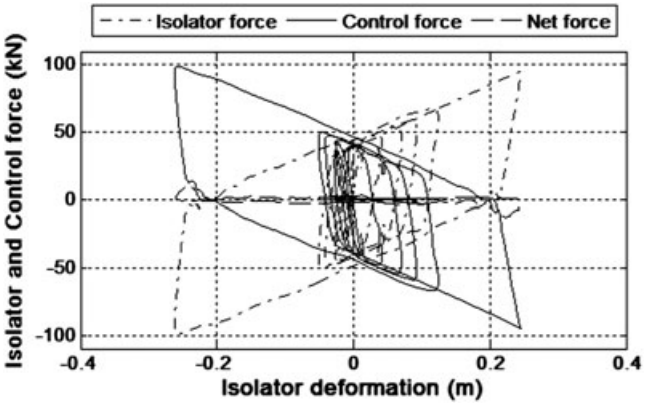

FIGURE 8 Sample isolator deformation versus isolator/control force deformation response; *Cont-C2* case under NF03 ground motion

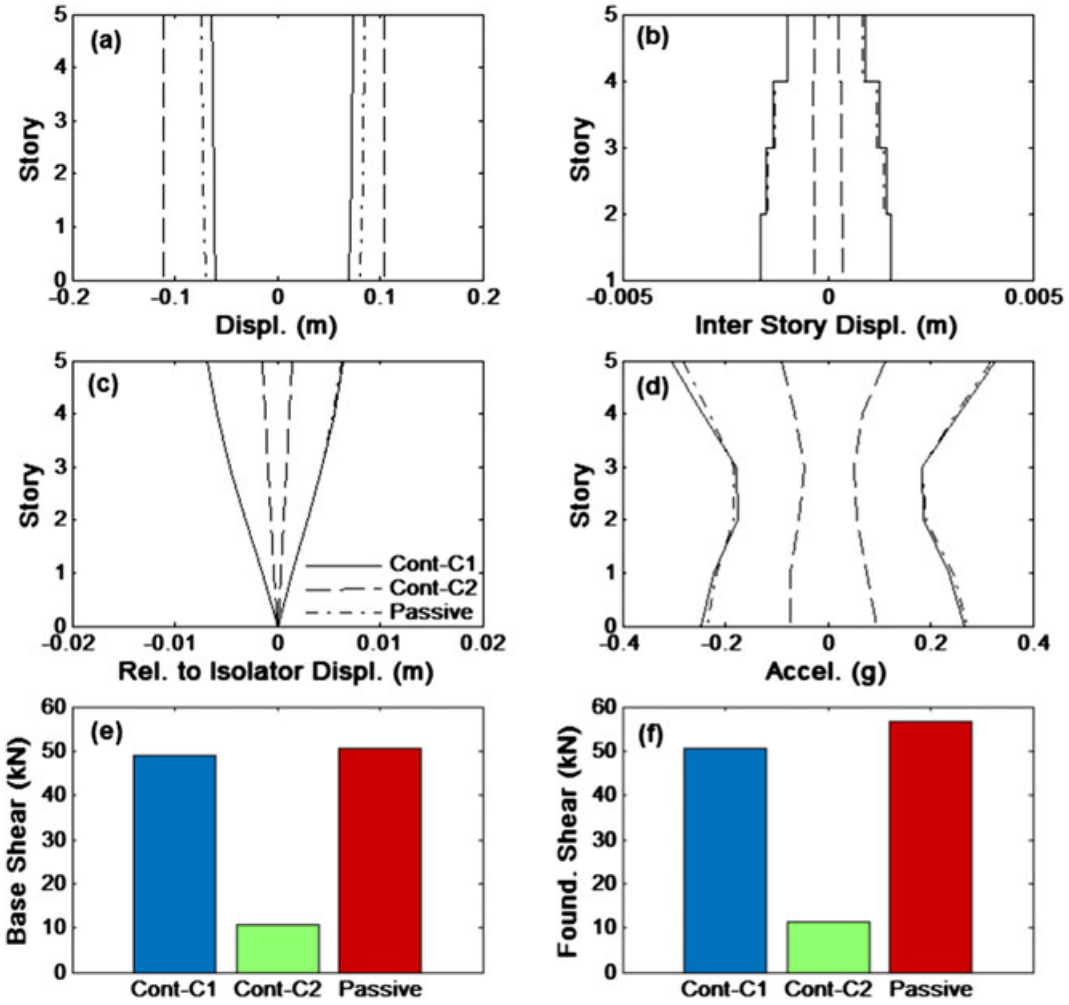

FIGURE 9 Comparison of average maximum response—far-field ground motions. (a) Story and base [isolator] displacements, (b) interstory drifts, (c) displacements relative to isolator, (d) story and base [isolator level] accelerations, (e) [superstructure] base shear, (f) sum of isolator force and control force (if any)

TABLE 3 Normalized response comparisons

	Near-field					Far-field				
	Cont-C1	**Cont-C1 + Noise**	**Cont-C2**	**LQG**	**PI**	**Cont-C1**	**Cont-C1 + Noise**	**Cont-C2**	**LQG**	**PI**
+ve isolator displ	0.625	0.612	1.383	1.018	0.947	0.868	0.836	1.298	1.304	1.094
-ve isolator displ	0.660	0.624	1.012	1.307	1.123	0.860	0.830	1.586	1.278	1.239
+ve story displ*	0.662	0.620	0.122	0.516	0.650	1.027	1.058	0.234	0.339	0.345
-ve story displ*	0.678	0.643	0.138	0.613	0.723	1.004	1.015	0.212	0.311	0.356
+ve story drift	0.760	0.739	0.311	0.516	0.650	1.078	1.099	0.320	0.339	0.345
-ve story drift	0.755	0.777	0.251	0.613	0.723	1.023	1.033	0.347	0.311	0.356
+ve story accel	0.755	0.778	0.267	0.609	0.719	1.023	1.032	0.348	0.298	0.343
-ve story accel	0.760	0.740	0.312	0.517	0.653	1.078	1.099	0.334	0.323	0.328
Peak base shear	0.643	0.596	0.119	0.613	0.723	0.973	0.987	0.212	0.336	0.356
Peak found shear	0.618	0.560	0.108	0.628	0.738	0.894	0.895	0.199	0.362	0.381

*Relative to isolators

Similar observations can be made in case of far-field (FF) ground motions. However, WNN-based control does not lead to significant changes in response quantities when compared to the conventional isolated system. This is primarily due to the fact that the passive isolator properties were deemed near optimal to achieve small displacements, accelerations, hence small forces, particularly for moderate level earthquakes as is the case with the FF ground motions.[37] Evidently, the seismic demand on the isolated structure due to FF ground motions is relatively insignificant in comparison to NF ground motions (Figure 9). This is confirmed by the present study as the average maximum control force in *Cont-C2* remained less than 13 kN versus 40 kN of isolator force with approximately 8% reduction in base displacements only. Finally, *Cont-C2* implementation resulted in significant reduction of all response quantities except for increased base displacements. Clearly, this may be considered a desired outcome as the benefits of reduced floor accelerations and interstory drifts outweigh the slight increase in the base displacements for certain types of buildings with deformation and acceleration sensitive equipment.

To demonstrate the relative efficiency as well as the effect of potential noise in the output measurements (acceleration response), additional cases were considered and simulated as listed in Table 3. The table summarizes normalized response quantities with respect to the conventional passive case. It can be seen that classical LQG and multivariable PI controllers can achieve the desired response reduction in general but fail to reduce deformation response at the isolation bearing level. In contrast, the achieved response reductions of all quantities by the Cont-C1 case with and without noise are similar, demonstrating the insensitivity of the proposed WNN-based controller to the noise in the measurements.

6 | SUMMARY AND CONCLUSIONS

The primary objective of this study was to assess the applicability of the proposed WNN-based control to reduce the isolator deformations (base displacements) in seismically isolated structures subjected to near-field ground motions. This can be achieved using conventional techniques by providing higher levels of damping at the isolation level but only at the expense of increasing floor accelerations and interstory drifts. Clearly, given the uncertainty and variability of ground motion characteristics, the control and reduction of both the displacements and accelerations require active control. For this purpose, a WNN comprising a wavelet back propagation network in parallel with a feedforward component trained using recursive least squares is introduced. The feedforward component significantly reduces the number of hidden layer nodes and provides fast efficient learning. The computational complexity of the error backpropagation algorithm is $O(n^3)$ with n hidden layer nodes. Consequently, the computational complexity of the wavelet neural network is reduced drastically with the number of hidden layer neurons. Hence, the parallel wavelet network is suited to online identification and control. The WNN-based control with MPC was used for online identification and control of a nonlinear structural system. The only input to the network was assumed to be monitored floor accelerations.

The efficacy of the method was demonstrated through a series of computational simulations. Two control cases that reduce the acceleration response and mitigate deformations were evaluated. Both cases demonstrate the effectiveness of WNN-based control in comparison to conventional isolation. They also highlight the efficiency and flexibility of the proposed approach to

achieve multiple performance objectives. All response quantities were significantly reduced for both near-field (NF) and far-field (FF) ground motions, in particular an average of 40% reduction in isolator deformations, with corresponding reductions in floor accelerations, was observed. A comparison between the average responses to NF and FF ground motions suggests that one of the control cases is capable of reducing large base displacements due to NF ground motions without compromising performance under FF ground motions.

The controller performance was dictated by the established performance objective through a penalty factor and WNN learning rate. The controller effectively regulated the apparent stiffness at the isolation level. This observed feature of the WNN-based control makes the method a desirable hybrid seismic isolation alternative in general and, particularly, a good candidate for lightweight structural system and equipment isolation. Finally, the proposed control method is fast, accurate, and robust, which allows implementation for large-scale dynamic systems. Furthermore, controllers that optimize other performance indices (objectives) can be readily implemented to provide more targeted response control.

ACKNOWLEDGEMENT

This study was funded in part by the Departments of Civil and Environmental Engineering, and Electrical and Biomedical Engineering at the University of Nevada, Reno, USA.

REFERENCES

[1] I. G. Buckle, R. L. Mayes, *Earthq. Spectra* **1990**, *6*, 161.

[2] F. Naeim, J. M. Kelly, *Design of Seismic Isolated Structures: From Theory to Practice*, John Wiley & Sons, Canada **1999**.

[3] J. F. Hall, T. H. Heaton, M. W. Halling, D. J. Wald, *Earthq. Spectra* **1995**, *11*, 569.

[4] R. S. Jangid, J. M. Kelly, *Earthq. Eng. Struct. Dyn.* **2001**, *30*, 691.

[5] I. G. Buckle, *Nucl. Eng. Des.* **1985**, 313.

[6] J. M. Kelly, *Earthq. Eng. Struct. Dyn.* **1999**, 3.

[7] J. M. Kelly, G. Leitmann, A. G. Soldatos, *J. Optim. Theor. Appl.* **1987**, *53*(2), 159.

[8] J. A. Inaudi, J. M. Kelly, *Earthq. Eng. Struct. Dyn.* **1993**, *22*, 297.

[9] S. Nagarajaiah, M. A. Riley, A. M. Reinhorn, *J. Eng. Mech.* **1993**, *119*(11), 2317.

[10] A. H. Barbat, J. Rodellar, E. P. Ryan, N. Molinares, *Eng. Mech.* **1995**, 676.

[11] N. Makris, *Earthq. Eng. Struct. Dyn.* **1997**, 571.

[12] M. D. Symans, G. L. Madden, A. N. Wongprasert. Experimental study of an adaptive base isolation system for buildings. *Proceedings of Twelfth World Conference on Earthquake Engineering* 2000, Auckland, New Zealand, **1965**.

[13] G. J. Madden, A. N. Wongprasert, M. D. Symans, *Comput. Aided Civ. Inf. Eng.* **2003**, 19.

[14] M. Usman, S. H. Sung, D. D. Jang, H. J. Jung, J. H. Koo. Numerical investigation of smart base isolation system employing MR elastomer. *Proceedings of the 11th Conference on Electrorheological Fluids and Magnetorheological Suspensions* **2009**.

[15] M. M. A. Salem, G. Pekcan, A. Itani. Seismic response control of structures using semi-active and passive variable stiffness devices. *Technical Report No: CCEER 14-01*, Center for Civil and Earthquake Engineering, University of Nevada Reno **2014**.

[16] M. Behrooz, S. Yarra, D. Mar, N. Pinuelas, B. Muzinich, N. G. Publicover, G. Pekcan, A. Itani, G. Gordaninejad. A self-sensing magnetorheological elastomer-based adaptive bridge bearing with a wireless data monitoring system, *Proc. SPIE 9803, Sensors and Smart Structures Technologies for Civil, Mechanical, and Aerospace Systems* **2016**, 98030D (April 20, 2016); https://doi.org/10.1117/12.2218691

[17] H. Chen, G. Tsai, J. Qi, F. Yang, F. Amini, *J. Comput. Civ. Eng.* **1995**, *9*(2), 168.

[18] J. Ghaboussi, A. Joghataie, *J. Eng. Mech.* **1995**, *121*(4), 555.

[19] K. Bani-Hani, J. Ghaboussi, *J. Eng. Mech.* **1998**, *124*(2), 319.

[20] D. A. Liut, E. Matheu, M. Singh, D. Mook, *Earthq. Eng. Struct. Dyn.* **1999**, *28*, 1601.

[21] H. J. Lee, G. Yang, H. Jung, B. Spencer, I. Lee, *Struct. Control Health Monit.* **2006**, *13*, 682.

[22] S. Suresh, S. Narasimhan, S. Nagarajaiah, N. Sundararajan, *Eng. Struct.* **2010**, *32*(8), 2477.

[23] S. Suresh, S. Narasimhan, S. Nagarajaiah, *Struct. Control Health Monit.* **2012**, *19*, 370.

[24] Y. Ohtori, R. E. Christenson, B. F. Spencer, S. J. Dyke, *J. Eng. Mech. ASCE* **2004**, *130*(4), 366.

[25] F. Allgöwer, A. Zheng, *Nonlinear model predictive control*, Birkhäuser, Basel **2000**.

[26] M. Han, W. Guo, J. C. Wang, *IEEE Inte. Joint. Conf. Neural. Netw.* **2005**, *4*, 2266.

[27] Q. Zhang, A. Benveniste, *IEEE Trans. Neural Netw.* **1992**, *3*, 889.

[28] C. C. Sousa, E. M. Hemerly, R. K. H. Galvao, *IEEE Trans. Syst. Man Cybern.* **2002**, *32*, 493.

[29] M. Zayeni, H. Ahmadi. Nonlinear system identification using radial wavelet networks. *Paper presented at SIAM meeting, St. Louis, Miss* **1995**.

[30] H. Khodabandehlou, M. S. Fadali. Networked control of unmanned vehicle using wavelet based GPC. *Paper to be presented in WCCI* **2016**.

[31] T. E. Saaed, G. Nikolakopoulos, J. E. Jonasson, H. Hdlund, *J. Vib. Control.* **2013**, *21*(5), 919.

[32] S. Kozák, *J. Electr. Syst. Informat. Technol.* **2014**, *1*, 1.

[33] G. J. Sirca, H. Adeli, *Scienta Iranica Trans. A: Civ. Eng.* **2012**, *19*(6), 1355.

[34] S.-L. Hung, C. S. Huang, C. M. Wen, Y. C. Hsu, *Comput. Aided Civ. Inf. Eng.* **2003**, *18*, 356.

[35] B. A. Anderson, J. B. Moore, *Optimal Control: Linear Quadratic Methods*, Prentice-Hall, New Jersey **1990**.

[36] J. Kelly, H. C. Tsai, *Earthq. Eng. Struct. Dyn.* **1985**, *13*, 711.

[37] J. C. Ramallo, E. A. Johnson, B. F. Spencer, *Eng. Mech.* **2002**, *128*(10), 1088.

[38] F. Ikhouane, J. Rodellar, *Systems with hysteresis, analysis, identification and control using the Bouc-Wen Model*, John Wiley & Sons, Ltd, Chichester, UK **2007**.

[39] MATLAB. Version 8.3.0.532 (R2014a). The MathWorks Inc., Natick, Massachusetts.

[40] FEMA. Quantification of building seismic performance factors. *Technical report, FEMA P695*. Prepared by Applied Technology Council for the Federal Emergency Management Agency, Washington, D.C. **2009**

How to cite this article: Khodabandolehlou H, Pekcan G, Fadali MS, Salem MMA. Active neural predictive control of seismically isolated structures. *Struct Control Health Monit*. 2017;e2061. https://doi.org/10.1002/stc.2061